Heliyon 9 (2023) e15977

Contents lists available at ScienceDirect

Heliyon

journal homepage: www.cell.com/heliyon

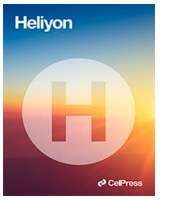

Research article

Hybrid gold-silica nanoparticles for plasmonic applications: A comparison study of synthesis methods for increasing gold coverage

Romain Trihan [a,*], Oskar Bogucki [b], Anna Kozlowska [b], Martin Ihle [c], Steffen Ziesche [c], Bartosz Fetliński [d], Bartosz Janaszek [d], Marcin Kieliszczyk [d], Marcin Kaczkan [d], Fabrice Rossignol [a], Anne Aimable [a]

[a] Univ. Limoges, CNRS, IRCER, UMR 7315, F-87000 Limoges, France
[b] Łukasiewicz Research Network – Institute of Microelectronics and Photonics, Al. Lotników 32/46, 02-668 Warsaw, Poland
[c] Fraunhofer Institute for Ceramic Technologies and Systems (IKTS), Winterbergstr. 28, 01277 Dresden, Germany
[d] Warsaw University of Technology – Institute of Microelectronics and Optoelectronics, 75 Koszykowa Street, 00-662 Warsaw, Poland

ARTICLE INFO

Keywords:
Heteroaggregation
Localized surface plasmon resonance (LSPR)
Silica
Gold
Nanoparticle
Microwave

ABSTRACT

The current work focuses on the synthesis of hybrid nanoparticles (NPs) made of a silica core (Si NPs) coated with discrete gold nanoparticles (Au NPs), which exhibit localized surface plasmon resonance (LSPR) properties. This plasmonic effect is directly related to the nanoparticles size and arrangement. In this paper, we explore a wide range of size for the silica cores (80, 150, 400, and 600 nm) and for the gold NPs (8, 10, and 30 nm). Some rational comparison between different functionalization techniques and different synthesis methods for the Au NPs are proposed, related to the optical properties and colloidal stability in time. An optimized, robust and reliable synthesis route is established, which improves the gold density and homogeneity. The performances of these hybrid nanoparticles are evaluated in order to be used in the shape of a dense layer for pollutant detection in gas or liquids, and find numerous applications as a cheap and new optical device.

1. Introduction

Environmental cause has become of major influence in our human society since a few decades [1], leading to an increase of regulations in many different fields, such as the control of pollutants in water, in air, and tolerance of some elements in pharmaceutics or in the food industry.

With the increase of standard requirements, it has been necessary to improve technologies and disposal for detecting chemical

Abbreviations: APTES, 3-aminopropyltriethoxysilane; BSPP, Bis(p-sulfonatophenyl)phenylphosphine; DP, Deposition Precipitation method; FRET, Förster Resonance Energy Transfer; KBH_4, Potassium Borohydrate; LSPR, Localized Surface Plasmon Resonance; $NaBH_4$, Sodium Borohydrate; NPs, Nanoparticles; PTT, Photo Thermal Therapy; PVP, Poly(vinyl pyrrolidone); SEM, Scanning Electron Microscopy; SERS, Surface-Enhanced Raman Scattering; SPR, Surface Plasmon Resonance; TA, Tannic Acid; TEM, Transmission Electron Microscopy; TEOS, Tetraethyl orthosilicate; TPP, Triphenylphosphine.

* Corresponding author.
E-mail address: romain.trihan@unilim.fr (R. Trihan).

https://doi.org/10.1016/j.heliyon.2023.e15977
Received 22 March 2023; Received in revised form 25 April 2023; Accepted 28 April 2023
Available online 6 May 2023

elements in the form of traces, directly on site and in a shorter range of time.

In such a context, optical devices represent a good choice for rapid detection of pollutants and device durability in time. For example, sensors based on Surface-Enhanced Raman Scattering (SERS) are currently developed to be used for food safety and environmental monitoring [2], as well as for biological detection [3]. Surface Plasmon Resonance (SPR), and in particular Localized Surface Plasmon Resonance (LSPR), is advantageous in improving detection sensitivity [4–8] and allows to detect analytes or molecules in the medical field as well [5,7–15].

To extend their use to new applications and improve their performances, research studies are conducted on the development of novel plasmonic materials and on improving their architecture [6,16–22]. LSPR nanoparticles are advantageous materials in the field of water disinfection [23] and in photothermal therapy (PTT) [24]. The materials used are usually gold [4,16,25], silver [2,11,26–29], aluminum [30], platinum [30], palladium [31] and more recently also vanadium oxide [32].

Gold colloids were first discovered by Faraday [33] and are usually synthesized from gold chloride as a precursor with sodium citrate, as first proposed by Turkevich et al. [34] and later refined by Frens [35]. In this synthesis, trisodium citrate is either a catalyst in the reaction or a dispersant [36]. Other dispersants can be used for nanoparticles stability, for example triphenylphosphine (TPP), bis(*p*-sulfonatophenyl)phenylphosphine (BSPP) and polymers such as poly(vinyl pyrrolidone) (PVP) [21].

Sodium borohydrate ($NaBH_4$) is usually used in growing the existing gold nanoparticles, as it is a strong reducing agent [37] and is similar to potassium borohydrate (KBH_4) for the synthesis of silver nanoparticles [38]. As most synthesis methods are using different steps for growing the nanoparticles, there is also existing methods to produce large gold nanoparticles in a single step [39].

Many other methods exist in the literature for the synthesis of gold NPs, such as microwave heating. Nevertheless, a domestic microwave does not allow a good control on the heating temperature and stirring is not possible in that case [40]. On the other hand, when using research-dedicated microwave equipment, the temperature is controlled in a better way, even though the size and morphology of the synthesized gold nanoparticles are not precisely controlled [41].

Previous work from Duff & Baiker [42] showed the possibility to achieve size-controlled gold seeds of 1–2 nm and later gold clusters in the range of 3–10 nm, when boiling the sol at quite high temperature (300 °C). Martin et al. [43] showed synthesis conditions to achieve almost monodisperse gold nanoparticles in water, however it requires a precise control of the concentrations of ions. More recent study from Piella et al. [44] showed the synthesis of size-controlled gold nanoparticles with the use of tannic acid (TA) in a quite well-controlled manner.

Concerning the optical properties, the LSPR peak position depends on the particle size [13,34] and also on the particle morphology. Indeed, for gold, the plasmonic signature is different according to the shape for nanorods [39,45], nanoshells [46,47], nanocages [48], losanges/bipyramids [49], nanocubes [39,45] or also nanostars [50,51].

Finally, the plasmonic properties also depend on the nanoparticles arrangement. NPs can be supported onto functionalized substrates or other supports like silica nanoparticles, which is a quite cheap material, easy to functionalize to get different reactive groups (amino, thiol, etc.) [38,52–54]. The Stöber method is well-known to allow producing spherical and monodisperse silica nanoparticles [55], which are able to make self-organized deposits onto substrates to achieve single-crystals with a significant number of layers [56].

Plasmonic nanoparticles in a core-shell structure, with an external silica shell and a gold core [39,57–61], are also of a great interest for other applications such as secondary plasmonic layer or FRET transfer [62,63]. With a silica shell, it can be functionalized, deposited onto substrates and self-organized into colloidal crystals with a large number of layers [56,60]. However, the silica shell is also responsible of a decrease in the optical properties and can shift the LSPR band due to refraction, depending on the shell thickness [64]. Moreover, it can result in a decrease of efficiency in detecting analytes.

The inverse configuration is also found with a silica core and a gold shell. That configuration is usually achieved using the deposition precipitation (DP) method [65–67], which consists of seeding gold grains onto the silica surface, then to make them grow in a second step. The nucleation step seems to cover homogeneously the surface of the silica particles but usually the LSPR band cannot be seen with gold grains that are too small (<2 nm). The growing step aims to adjust the gold size and so the LSPR peak position and intensity. Nevertheless, it is not so easy to control the reaction of growing the seeds together with avoiding coalescence [68–70], which might result in a plasmon signature with a broad band.

Another way to functionalize silica particles with gold particles is heteroaggregation, that consists in aggregating particles of opposite charge. Since the first work of Halas et al. [71] some references are found in the literature for gold-silica nanoparticles [38,61,68,70,72–74]. Nevertheless, it appears difficult to control the density and homogeneity of gold coverage onto the silica particles with experimental reproducibility [69,75–77].

Regarding the extent of literature, our original study compares in a rational approach different synthesis routes for the synthesis of hybrid nanoparticles made of silica cores covered by gold nanoparticles, based on nucleation-growth and heteroaggregation. Microwave experiments are also presented, in order to have a better control on the temperature and improve the reaction kinetics. Different sizes of silica and gold nanoparticles are synthesized to study their influence on the coverage density. We give many importance to the criterion of reproducibility and experimental reliability to propose an optimal synthesis of silica-gold nanoparticles, which could be easily transferred to an industrial process, and become the basis of a new optical plasmonic device exploiting LSPR detection.

2. Experimental section

2.1. Materials

The reagents used for the synthesis of silica nanoparticles include tetraethyl orthosilicate (TEOS, 98%, Acros Organics), ammonia

hydroxide (NH_4OH, 28–30 wt%, Acros Organics), absolute ethanol (C_2H_5OH, VWR Chemicals) and deionized water (equipment Biopure 7/15 from Elga, 15 MΩ cm). The silane 3-aminopropyltriethoxysilane (APTES, 98%, Alfa Aesar) was used to functionalize the surface of the synthesized silica nanoparticles with an amino (-NH_2) terminal group.

The reagents used for functionalization with gold nanoparticles include hydrogen tetrachloroaurate (III) also called gold (III) chloride ($HAuCl_4$*x.H_2O, 99.9%, Alfa Aesar), sodium hydroxide (NaOH, anhydrous, ≥98%, Sigma Aldrich), trisodium citrate ($C_6H_5Na_3O_7$*2. H_2O, ≥99%, Fisher Scientific), sodium borohydrate ($NaBH_4$, 99%, Acros Organics) and potassium carbonate (K_2CO_3, 99%, Alfa Aesar).

Tannic acid (TA, Sigma Aldrich) was also used for the synthesis of gold nanoparticles. Hydrochloric acid (HCl, 36%, Alfa Aesar) was used in addition for zeta titration and for adjusting the pH of the silica nanoparticles solution.

2.2. Sample preparation

2.2.1. Silica nanoparticles synthesis

The silica nanoparticles were synthesized using conditions derived from the Stöber procedure [55,75,78]. In this sol-gel method, the hydrolysis and condensation of TEOS are controlled using different amounts of ammonia and deionized water. The different protocols and formulations are shown in Table 1. For Protocols 1 and 2 only, the ammonia is added directly to the TEOS/EtOH solution. For Protocols 3 and 4, the TEOS is first dispersed into half of the ethanol solvent and the other half is used to mix the ammonia and deionized water, before mixing the two solutions together. The resulting synthesis medium is kept for a fixed reaction time at room temperature under vigorous magnetic stirring (>300 rpm) while avoiding the evaporation of the solvent during that time.

The solution medium becomes white due to condensation of TEOS, leading to the formation of spherical silica nanoparticles. After reacting, the solution medium is centrifuged and washed in ethanol for 10 min at 6000 rpm for nanoparticles of 400 and 600 nm, or at 9000 rpm for nanoparticles of 80 and 150 nm. The washings are repeated for a total of 4 washing steps. The silica nanoparticle powders are retrieved after drying into a heat chamber.

2.2.2. APTES functionalization of the silica nanoparticles

The synthesized silica nanoparticles surface was functionalized with amino functions (-NH_2) using the APTES silane reagent. Typically, 1.48 g of silica nanoparticles are ultrasonically redispersed into 200 mL of deionized water, prior to the addition of 3.7 g of APTES. The solution is kept at room temperature for 24 h under gentle stirring (250–300 rpm), avoiding evaporation of solvent. The amount of APTES is the same whatever the particle size, as it is in excess compared to the added silica amount. The reaction is usually complete in less than 16 h.

After that, the reaction medium is centrifuged and washed with deionized water for 10 min at 6000 rpm for nanoparticles of 400 and 600 nm, or at 9000 rpm for nanoparticles of 80 and 150 nm. The washings are repeated for a total of 4 washing steps. Finally, the amine-functionalized silica nanoparticles are redispersed in 40 mL of deionized water.

2.2.3. Gold-seeding on silica nanoparticles: conventional heating with water bath

The gold-seeding procedure typically consists in using 0.3 g of amine-functionalized silica nanoparticles added to 20 mL of $HAuCl_4$ precursor (6.35 mM). The gold-seeding reaction is initiated by the addition of 4.5 mL of NaOH (0.1 M) leading to the formation of [AuCl(OH)3]- complex and beginning of the deposition-precipitation process. The protocol has been adjusted from previous work of Kah et al. [65,66] to afford homogeneous grafting of gold onto the silica nanoparticle surface and avoiding premature growing of the grains. Two kinetics conditions have been chosen with a water bath as the heat source: (i) 65 °C for 30 min or (ii) 90 °C for 15 min.

The obtained orange-brown coloration indicates loading of $Au(OH)_3$ nanoparticles on the amine-functionalized silica nanoparticles. For purification, the solution of gold-seeded silica nanoparticles was centrifuged and washed with deionized water at 1000 rpm for 10 min for a total of 8 washings. The gold-seeded silica particles were then redispersed into 40 mL of deionized water.

2.2.4. Gold-seeding on silica: microwave controlled-system heating

The tests performed with microwave heating aimed at improving density of the gold grains onto the silica surface during the gold-seeding reaction. These experiments consisted of a microwave irradiation under magnetic stirring in a multimode microwave oven (Ethos 1600 MicroSynth, Mileston). Temperature was measured with a ATC-FO/Ethos fiber-optic thermometer. Two heating conditions were chosen and adapted from the conditions with conventional heating: (i) 65 °C, 100 W, 30 min and (ii) 90 °C, 200 W, 15 min.

Table 1
Synthesis conditions (Stöber procedure) to achieve different sizes of silica nanoparticles.

SYNTHESIS	Protocol 1		Protocol 2		Protocol 3		Protocol 4	
Targeted size	80 nm		150 nm		400 nm		600 nm	
	wt%	mol%	wt%	mol%	wt%	mol%	wt%	mol%
TEOS	1.58	0.35	1.58	0.34	2.01	0.37	9.85	1.67
EtOH	92.56	91.99	90.95	88.23	76.99	63.70	61.03	46.78
Ammonia 28%	5.86	7.66	5.89	7.49	8.26	8.98	5.76	5.80
Deionized water	–	–	1.58	3.94	12.74	26.95	23.36	45.75
Reaction time (h)	24		24		24		16	

The fluctuation of temperature registered using the automatic controlled system was <1 °C. Purification was carried out by centrifugation the same way as for the other gold-seeding reactions (washings with deionized water at 1000 rpm for 10 min for a total of 8 washings).

2.2.5. Gold-growing on gold-seeded silica nanoparticles

For growing the gold-seeds, a gold precursor solution is prepared by diluting 1.5 mL of $HAuCl_4$ at 25 mM in 100 mL of deionized water and adding 60 mg of K_2CO_3. This solution is left overnight under gentle magnetic stirring (typically 250 rpm) and is later referred to as K-gold solution. From the work of Kah et al. [65,66], it appeared beneficial to choose a K-gold/silica volume ratio of 5:1 to avoid coalescence of the grains and guarantee that the LSPR band would be as sharp as possible. In other words, after having ultrasonically redispersed the gold-seeded silica solution (equivalent concentration than 0.3 g of amine-functionalized silica in 40 mL deionized water), 5 mL were added to 25 mL of K-gold solution. The gold-growing reaction was then initiated by adding 3 mL of a freshly prepared solution of $NaBH_4$ (6.6 mM). Indeed, the solution became red in a few seconds after adding the reducing agent $NaBH_4$. The solution was kept for a minimum of 6 h with gentle stirring (~200 rpm) to ensure complete reaction.

For purification, it appeared beneficial to choose to retrieve the particles using filtration instead of centrifugation. Indeed, using centrifugation for a long time and at a high rotating speed would increase the possibility to detach the gold grains from the silica surface, due to friction in between the particles. Filtration was then performed by diluting the reaction medium in a large amount of deionized water and using a 0.22 μm membrane (mixed cellulose ester membranes from MF-Millipore). This filtration method was appropriate to retrieve silica-gold particles of a size higher than 220 nm and with filtering smaller particles (like possible detached gold grains in the reaction medium).

2.2.6. Gold nanoparticles synthesis

The synthesis of gold NPs was performed according to the sequential protocol described by Bastús et al. [79]. Briefly, a gold seeds solution is achieved by adding 1 mL of $HAuCl_4$ (25 mM) into 150 mL of trisodium citrate (2.2 mM) at 100 °C. The solution becomes pink due to the seeds formation. Once the reaction is finished, the mixture is cooled down to 90 °C and growing of the seeds is achieved by successive additions of 1 mL of trisodium citrate (60 mM) and 1 mL of $HAuCl_4$ (25 mM). In this work, gold nanoparticles were prepared up to 8 additional steps.

Another procedure has been tested to achieve highly monodisperse Au NPs of a smaller size, adapted from the work of Piella et al. [44]. The difference is that tannic acid helps stabilizing the size of the gold seeds. Briefly, 0.1 mL of tannic acid (2.5 mM) and 1 mL of K_2CO_3 (150 mM) are added into 150 mL of sodium citrate (2.2 mM) at 70 °C. The gold seeds solution is achieved by adding 1 mL of $HAuCl_4$ (25 mM). Once the reaction is finished, growing of the seeds is achieved by successive additions of 0.5 mL of sodium citrate (2.2 mM) and 0.5 mL of $HAuCl_4$ (25 mM). In this work, these gold nanoparticles were prepared up to 16 additional steps.

2.2.7. Heteroaggregation: grafting gold nanoparticles onto amine-functionalized nanoparticles

Heteroaggregation consists of aggregating particles of opposite charge. Raw silica particles are usually negatively charged in the working range of pH (>3) but so do the gold nanoparticles stabilized with trisodium citrate. Modification of the silica surface charge is performed by APTES functionalization described previously and allow to target a positive charge for the amine-functionalized silica (with adjusting the working pH if needed).

As the silica nanoparticles have different sizes (and different BET surfaces), it is necessary to adjust the quantity of silica nanoparticles added to the as-synthesized gold nanoparticles. Typically, amine-functionalized silica particles are redispersed into deionized water (at a concentration of 700 mg in 40 mL). A volume of 100–200 μL is added to 1 mL of the Au NPs solution and these additions are repeated to get the desired volume, in the same order of addition to guarantee an homogeneous coverage. Indeed, considering a big volume of silica added to the gold solution, the first drops of silica would be totally covered and the last drops would be less covered.

For the purification procedure, washings consist of letting the gold-grafted silica nanoparticles sediment and remove the supernatant. Washings are repeated 4–5 times with deionized water. The sedimentation approach is preferred contrary to centrifugation procedures, in order to avoid removing the gold nanoparticles from the silica surface, due to friction in between the particles. After purification, the gold-grafted silica nanoparticles can be redispersed using ultrasound bath without risk of removing the gold nanoparticles from the surface.

2.3. Characterization & instrumentation

The nanoparticle density was measured using pycnometry, with an equipment AccuPyc II 1340 from Micromeritics (cell volume 1 cm^3, target pressure 19.500 psig, 10 measurements per sample).

BET (Brunauer-Emmett-Teller) surface area of the silica particles was quantified using an ASAP2020 from Micromeritics (degas condition of 90 °C for 30 min then 200 °C for 10 h, BET 8 points under nitrogen).

Zeta potential of nanoparticles was measured as a function of pH using a Zetasizer Nano series from Malvern, with a multi-purpose titrator MPT-2 (cell type DTS1060, 3 measurements with titrants HCl or NaOH at 0.1 M, range of pH 3.0–10.0, pH increment 0.5 and pH tolerance of 0.2, particle concentration 0.1 wt% in deionized water).

Images of the as-prepared silica nanoparticles were performed using Scanning Electron Microscopy (SEM) with a LEO 1530 equipment (1–5 kV, aperture 30 μm, working distance 3.00 mm). Observations were conducted without metallization of the particles.

Gold nanoparticles and gold-functionalized silica particles were observed using Transmission Electron Microscopy (TEM) on a JEOL 2100F equipment (200 kV).

Image analyses were done using the ImageJ freeware to extract the particle size distribution.

Optical response from the gold particle solutions, raw silica and gold-functionalized silica were measured using UV–visible with a Quickdrop spectrophotometer from Molecular Device (quartz cell, pathlength 10 mm, wavelength range 190–990 nm, measurement time 5 s). These measurements afford to see the LSPR absorption band (peak position and intensity).

3. Results and discussion

3.1. Characterization of the raw silica and amine-functionalized silica nanoparticles

All nanoparticles characteristics are gathered in Table 2, SEM pictures of the synthesized silica nanoparticles are shown in Fig. 1 (a–d). The size distribution and zeta potential curves are shown in Appendix (Fig. S1 & Fig. S2).

3.2. Gold-seeding reaction for different temperatures and different heating methods

For the preliminary experiments, only silica particles with a size of 400 nm were used. The reactions consist in reproducing the conditions used by Kah et al. [65,66], using a conventional water bath at different temperatures. The pictures of the reacted solutions

Table 2
Synthesis conditions and characteristics of the synthesized silica nanoparticles.

SYNTHESIS	Protocol 1	Protocol 2	Protocol 3	Protocol 4
Targeted size	80 nm	150 nm	400 nm	600 nm
Average Size (nm)	78 ± 8	156 ± 16	381 ± 27	599 ± 27
Number of particles (N)	523	500	415	424
S BET (m^2/g)	48.6 ± 0.8	21.9 ± 0.4	6.0 ± 0.3	5.7 ± 0.1
He Pycnometry (g/cm^3)	2.10	2.10	2.02	1.98
IEP of amine-silica	7.7	8.0	7.2	5.6

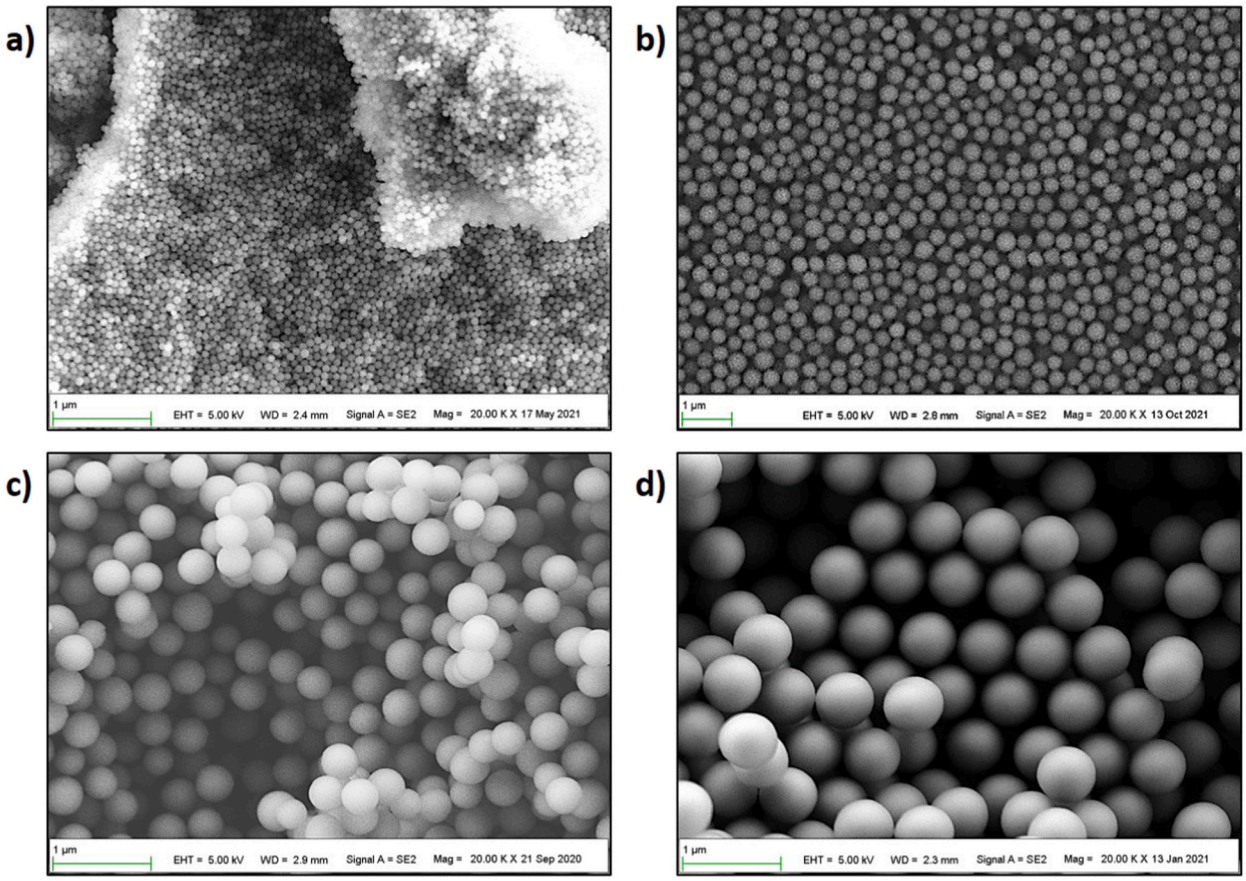

Fig. 1. SEM pictures of the synthesized silica nanoparticles of 80 nm (a), 150 nm (b), 400 nm (c) or 600 nm (d) with the same magnification.

are shown in Appendix (Fig. S3). Contrary to the results found by Kah et al., the reaction of gold-seeding appears only onto amine-functionalized silica particles and not onto raw silica particles (raw silica particles remain white after reaction). Moreover, the gold-seeding reaction conducted onto different batches of amine-functionalized silica particles shows different reaction efficiency, as one can deduce from the different supernatant coloration after centrifugation (Fig. S3). This emphasizes that this reaction might be not repeatable, which is to be avoided.

On the purpose to achieve a higher reaction efficiency and procedure repeatability, the conditions were repeated using microwave heating (laboratory microwave with control of the temperature). This kind of heating method affords a better temperature diffusion and homogeneity in the solution. After reaction, the reacted particles were centrifuged and retrieved for TEM observations (Fig. 2 (a–d)).

The TEM observations show an homogeneous and dense gold-seeding reaction for the particles prepared with 65 °C/30min under conventional heating (Fig. 2a). The same reaction conducted at 90 °C/15min shows a nucleation less homogeneous and less repeatable than the first condition tested. Indeed, some silica particles were not totally decorated with gold seeds (Fig. 2b). The same temperature used with microwave heating allows to get silica particles that are quite homogeneous and similarly grafted, but this conducted also to larger gold seeds aggregates, which is to be avoided (Fig. 2d). The microwave heating at 65 °C/30min shows less gold aggregates (Fig. 2c). Nevertheless, the gold seeds are quite dense and very close to one another, which might lead to a core-shell structure and not to the desired configuration of silica particles decorated with gold particles.

It appeared then that the microwave heating method is not advantageous to get more homogeneous gold-seeded silica particles, as it generates gold seeds aggregates. In addition, using a conventional water bath heating with temperature 90 °C/15min is not appropriate for reaction repeatability and it appeared that 65 °C/30min with conventional water bath is a better choice to get a smooth, repeatable and homogeneous reaction. This condition was chosen to conduct the experiments of growing gold onto the gold-seeded silica particles.

3.3. Standard gold-growing procedure using $NaBH_4$ precursor

The gold-growing reaction was conducted onto gold-seeded silica particles previously prepared at 65 °C/30min under conventional water bath heating. The procedure uses a K-gold solution and a freshly prepared $NaBH_4$ precursor solution, which aims to reduce the complex gold hydroxide anions in the K-gold solution onto the seeds, in order to make them grow. The K-gold/silica volume ratio is fixed to 5:1, on the one hand to allow enough growing for the detection of an LSPR peak position in UV–visible and on the other hand to avoid undesired coalescence [65].

When adding $NaBH_4$ to the K-gold solution, a fast color change occurs in a few seconds from milky white to dark red, as a sign of

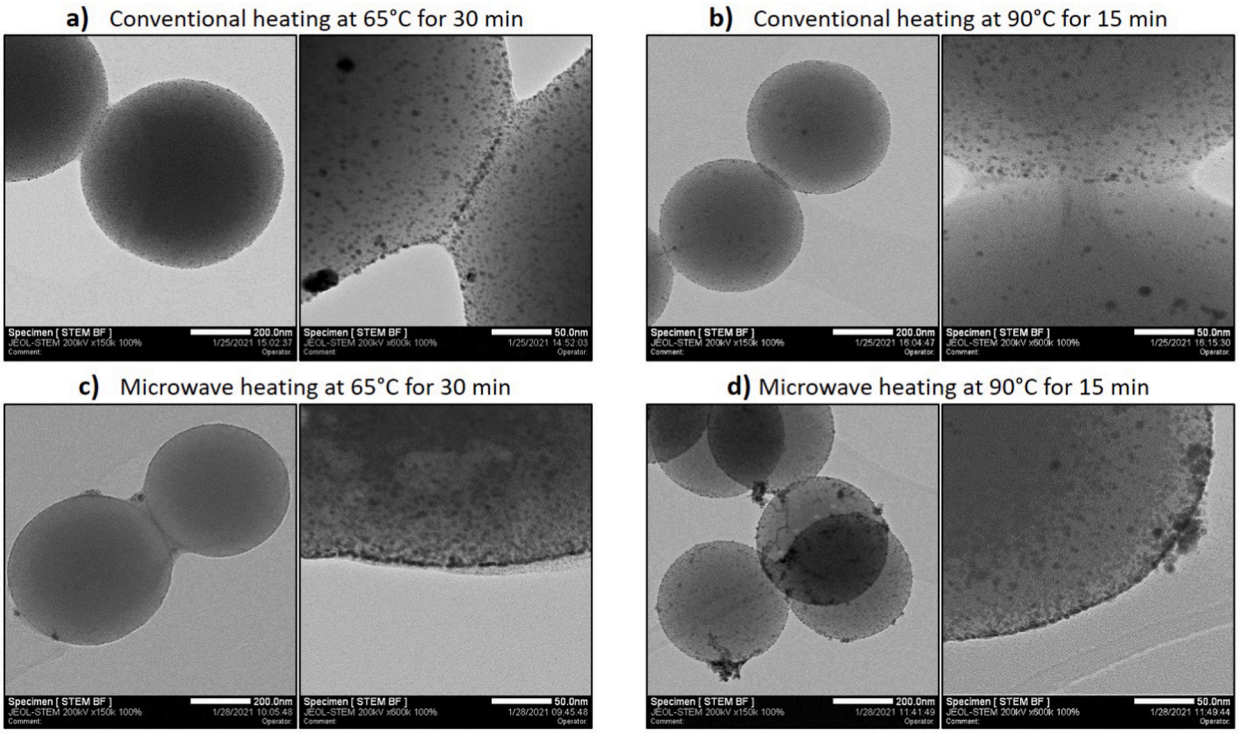

Fig. 2. TEM pictures of the gold-seeded silica particles under different conditions of temperatures and different heating methods (conventional water bath (a–b) or microwave heating (c–d)).

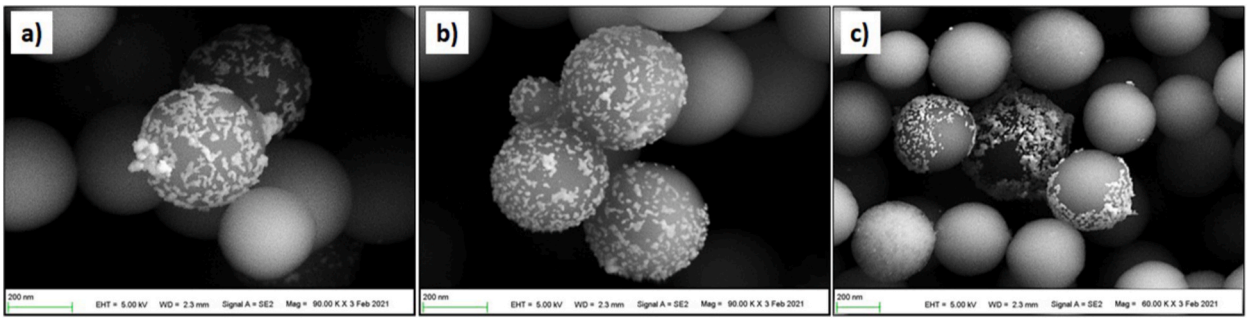

Fig. 3. SEM pictures of the nanoparticles obtained from the gold-growing procedure after filtration (a–c).

gold nanoparticles formation, which could also be attributed to growing of the seeds (increase of absorption). The solution was kept under stirring for about 6 h to complete the reaction. In order to avoid removing the gold grains from the silica surface, filtration (with filtration paper of 0.22 μm for silica nanoparticles of around 400 nm) was used rather than centrifugation. Washings were performed by diluting the solution in a large volume of deionized water. The filtration allowed to extract the nanoparticles and observe them using SEM, as shown in Fig. 3(a–c).

Previously, the gold-seeding reaction was quite homogeneous (Fig. 2a), although not exactly repeatable (Fig. S3). From the pictures of the particles after gold-growing, one can see that the reaction leads to the formation of gold aggregates and is not homogeneous and not repeatable onto the gold-seeded silica particles. This may be due to the fact that the reaction kinetics is extremely fast with the addition of the $NaBH_4$ component and leads to a lack of homogeneous growing.

From the obtained pictures, one might think that the K-gold/silica volume ratio should be increased and that the growing reaction might not be complete. As a control procedure to check if the reaction was complete, a sample volume of the reacted solution was extracted before filtration and observed in SEM after drying, as shown in Appendix (Fig. S4). Moreover, after filtration, as the filtered solution (filtrate) was of an intense red color, UV–visible characterization was performed and is also shown in Appendix (Fig. S4). The SEM picture (Fig. S4) shows the spherical silica nanoparticles into a solid network of smaller nanoparticles. These smaller nanoparticles are similar to gold nanoparticles, as confirmed with the UV–visible spectrum from the filtered solution, similar to the LSPR peak absorption of gold nanoparticles.

Indeed, the use of $NaBH_4$ in presence of a metallic precursor is responsible of an instant nucleation into the reaction medium and a fast formation of metal nanoparticles, as shown for silver nanoparticles by Agnihotri et al. [27]. Despite a low K-gold/silica volume

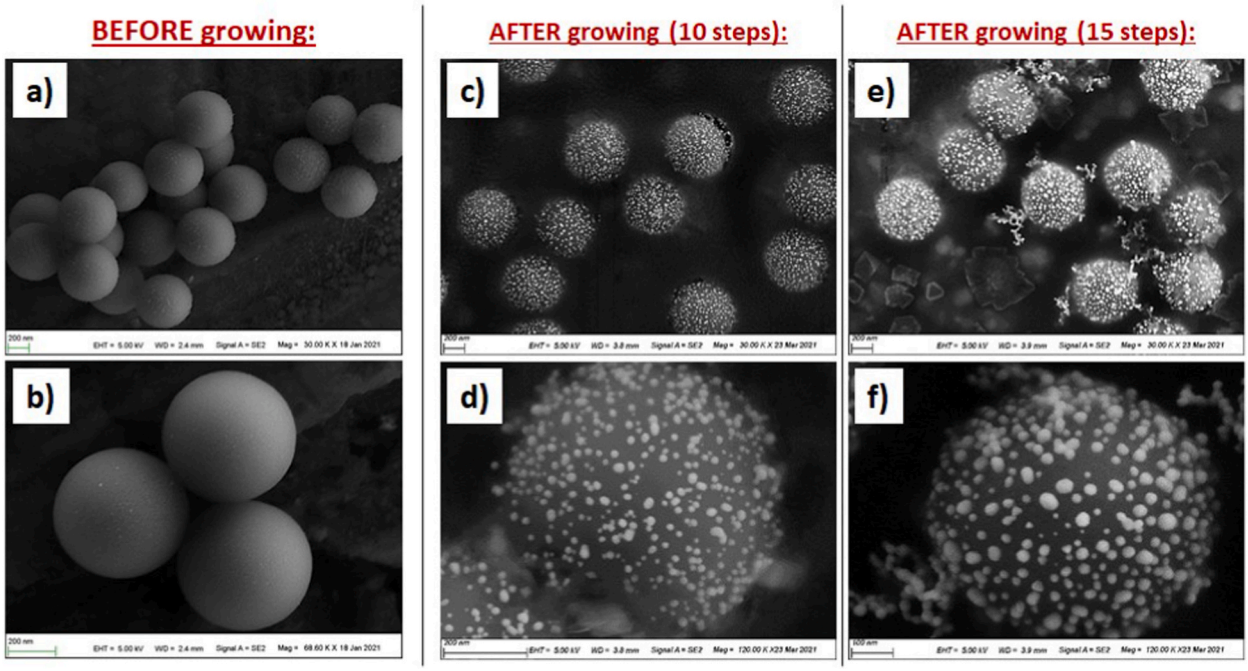

Fig. 4. Silica-gold nanoparticles achieved from the gold-seeded silica particles (a–b) with 10 (c–d) or 15 (e–f) successive additions of trisodium citrate and $HAuCl_4$ at 90°C (no centrifugation).

ratio of 5:1, the concentration of gold nanoparticles formed into the solution should have allowed growing of the gold seeds onto the silica nanoparticles. The low efficiency of this reaction can be attributed to a second role of the reducing agent $NaBH_4$, that is indeed a strong ligand [27]. This explains its high capacity to maintain the gold seeds shape, but leads on the other hand to a mismatch and absence of efficient reaction with the gold seeds onto the silica nanoparticles.

3.4. Gold-growing procedure using trisodium citrate

Trisodium citrate is a less strong ligand than $NaBH_4$ precursor, which might lead to a smoother gold-growing reaction of the gold seeds of interest. Conventional gold-growing procedure uses trisodium citrate, as in the procedure of growing gold nanoparticles [79]. This procedure might afford a better control of the reaction and the successive additions of trisodium citrate and $HAuCl_4$ would allow controlling the targeted size for the gold grains onto the silica particles. This procedure was used onto gold-seeded silica redispersed into trisodium citrate (2.2 mM) heated at 90 °C in a water bath and with 10 and 15 successive additions of trisodium citrate and $HAuCl_4$. During the procedure, smooth increase of the solution absorbance is observed (Fig. S5), which is in accordance to a growing of the gold grains on the silica particles. The washings performed after reaction using centrifugations confirmed that the gold grains were detached from the silica surface (Fig. S6). Observation of the reacted particles was then performed without centrifugation (Fig. 4(a–f)).

The SEM pictures of the reacted gold-silica particles show a clear increase in the gold grains size with increasing the number of additions of trisodium citrate and $HAuCl_4$. Moreover, the gold-growing procedure using trisodium citrate instead of $NaBH_4$ leads also to the formation of gold particles into the reaction medium, although on a much lower quantity. Even though this reaction is smooth and not fast, this leads to gold grains with a wide range of sizes, which is not quite appropriate for the application. However, the gold grains are still spaced with correct distance in between one another, which affords to avoid coalescence.

3.5. Synthesis of gold nanoparticles: stability of size, shape and stability in time

Another way to functionalize silica particles with gold grains is to graft gold nanoparticles directly onto the silica nanoparticles, using the heteroaggregation method. This has the advantage to have a sharp size distribution of the gold particles, contrary to the silica-gold particles achieved with the gold-seeding and gold-growing procedures. On the purpose to graft gold nanoparticles onto silica nanoparticles, different methods were explored for the gold nanoparticles synthesis.

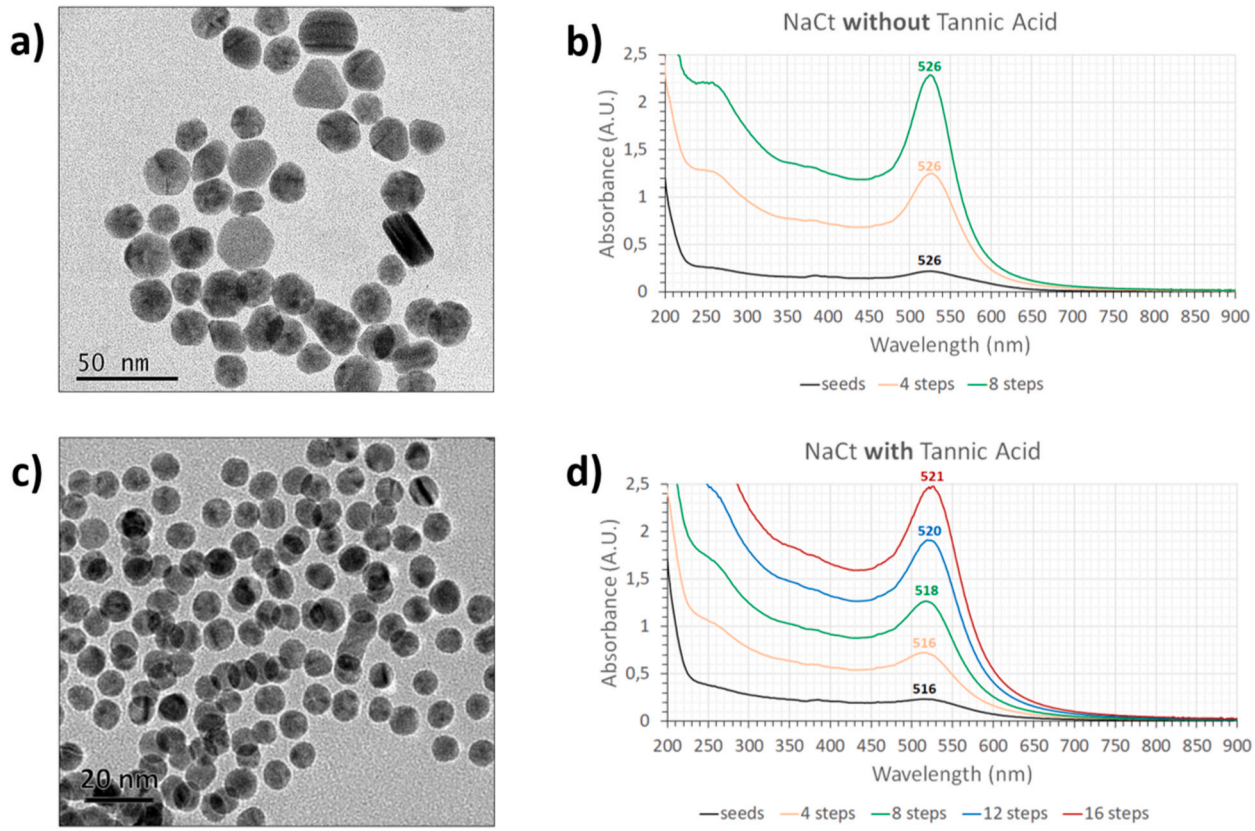

Fig. 5. TEM pictures of the gold particles synthesized and corresponding absorbance curves at different steps for the synthesis of gold particles without tannic acid (a) (b) and with tannic acid (c) (d) (The coalescence-like effect seen on picture (c) is due to the beam intensity during TEM observation).

The optical and LSPR properties are linked to the gold particles size. It is obvious and of a high important to be able to control the gold nanoparticles size, which was not possible with the previous method of gold-seeding and gold-growing. Moreover, the process needs to be repeatable and reproducible. A classical way to produce gold nanoparticles is to use only trisodium citrate with the gold precursor $HAuCl_4$ [79] and another way is to use tannic acid to have a better control on the gold nanoparticles shape and size [44]. The gold particles synthesized with these two procedures are shown in Fig. 2 with the corresponding absorbance curve at different growing steps to adjust the particle size and the LSPR band intensity.

Despite a good LSPR peak observed in UV–visible characterization (Fig. 5b), the shape and sizes of particles synthesized without tannic acid were not stable and not repeatable (Fig. 5a). Moreover, it was observed that these particles were not quite stable in time upon storage before use (see Appendix, Fig. S7). On the other hand, the use of tannic acid allows getting a narrow size distribution of the synthesized gold nanoparticles (Fig. 5c) and an intense LSPR peak, depending on the number of adding steps (Fig. 5d). The particles synthesized with the use of tannic acid are also more stable in time during storage before use (see Appendix, Fig. S8).

On the one hand, the synthesis procedure without tannic acid allowed achieving gold nanoparticles of roughly 30 nm. On the other hand, the synthesis of citrate-stabilized gold nanoparticles with the use of tannic acid allowed achieving gold nanoparticles of about 8.2 nm for 8 steps and 10.3 nm for 16 steps.

In solution, stability of the synthesized gold particles is correlated to the trisodium citrate content, as the citrate-stabilized gold nanoparticles are negatively charged in a wide range of pH (Appendix, Fig. S9). For these particles, the zeta potential is in between −34 mV and −60 mV on the range of pH in between 3.0 and 10.0. With such negatively charged particles, it is then possible to proceed to heteroaggregation onto amine-functionalized silica nanoparticles, which are positively charged (Fig. S2).

3.6. Gold-grafting through heteroaggregation method

Heteroaggregation consists of a fast interaction of particles with opposite charges. The higher the charge difference, the faster the reaction. The synthesized citrate-stabilized gold particles are negatively charged on the working range of pH (3.0–10.0) for all sizes of

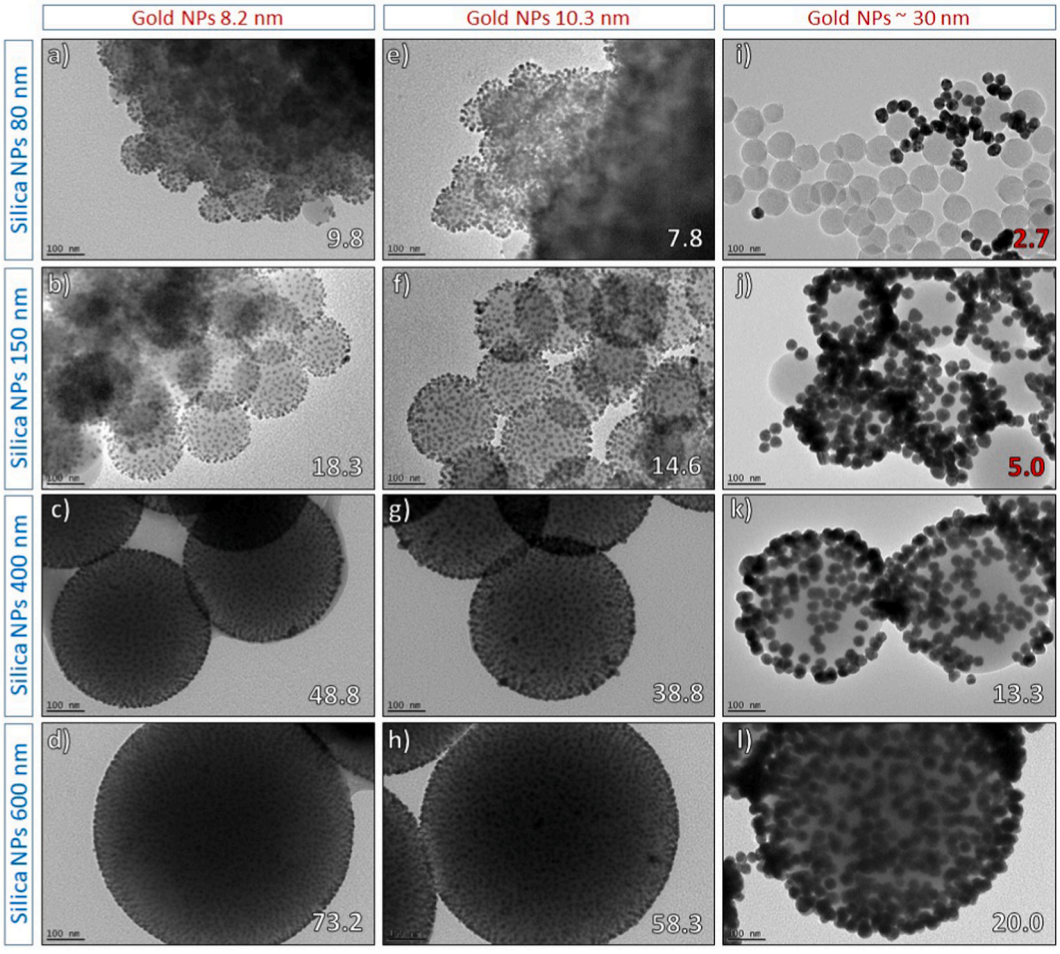

Fig. 6. TEM pictures of the gold-silica nanoparticles achieved with different sizes of silica NPs (80, 150, 400, 600 nm) for gold NPs of a size of 8.2 nm (a–d), 10.3 nm (e–h) or about 30 nm (i–l) The number given in the pictures corner is the particle size ratio silica/gold.

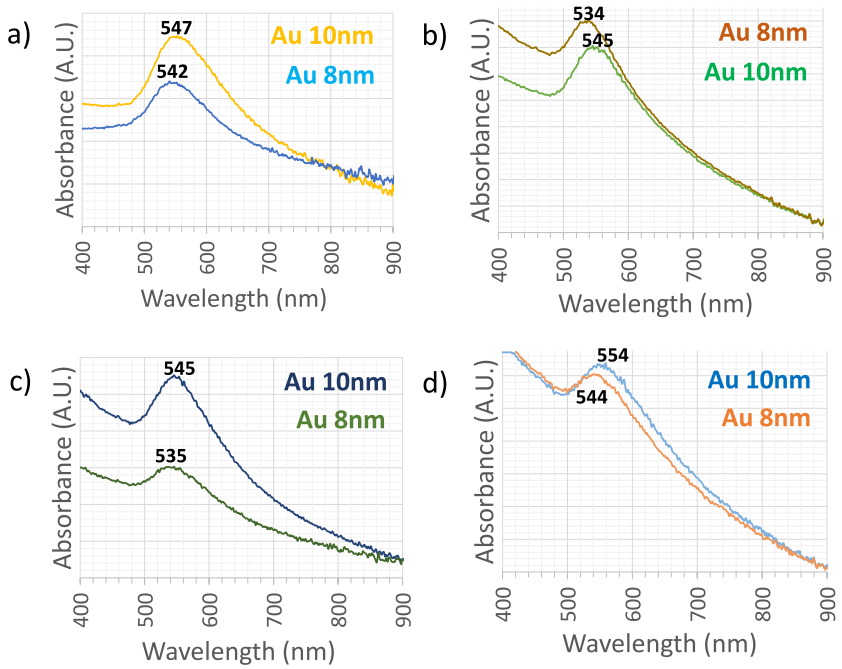

Fig. 7. Corresponding LSPR signature for gold nanoparticles (size 8.2 or 10.3 nm) deposited onto silica particles (size 80, 150, 400 or 600 nm).

particles (8.2 nm, 10.3 nm and about 30 nm). It is then possible to adjust the pH of the amine-functionalized silica nanoparticles in the appropriate range of pH (*i.e.* acidic pH) to have a positive charge (Fig. S2) and allow spontaneous grafting of gold nanoparticles onto the silica nanoparticles, for all sizes of silica nanoparticles (80 nm, 150 nm, 400 nm and 600 nm).

As the silica nanoparticles have different sizes, it was necessary to adjust the silica nanoparticles volume to add to the as-synthesized gold nanoparticles, according to their BET surface (Table 2). The obtained gold-silica nanoparticles are shown on the TEM pictures of Fig. 6(a–l).

The resulted gold-silica particles obtained appear very homogeneous and with a dense and smooth coverage of gold particles onto the silica particles, especially using small gold particles (8.2 and 10.3 nm, Fig. 6(a–h)). On the other hand, the use of larger gold particles (~30 nm) gave also quite a good coverage on big silica particles (600 nm and 400 nm, Fig. 6(k and l)) but not onto smaller silica particles (150 nm and even worse for 80 nm, Fig. 6(i and j)). This emphasizes an effect of the surface curvature. In other words, the particle size ratio silica/gold should be high enough to allow no curvature effect and guarantee a good grafting of the gold particles onto the silica surface. Based on the multiple gold and silica sizes tried, it seems that the particle size ratio silica/gold should be greater than 5.0 to guarantee a good coverage of the gold particles on the silica surface. In addition, it seems better for preparation repeatability to use gold particles of a small size.

The UV–visible curve of the as-prepared gold-silica LSPR particles were obtained (Fig. 7(a–d)). As the silica particles of different sizes have different absorption curves (Appendix, Fig. S10) and were used in different amounts, raw spectra (Appendix, Fig. S11) were normalized with the absorption values at 400 nm and 900 nm. For these measurements, the gold-silica particles were redispersed into deionized water to avoid the presence of specific ions and undesired LSPR shift. Additional TEM analyses showed no coalescence effect and no morphology changes of the gold particles after grafting onto the silica particles, even when the particles get in contact (see Appendix, Fig. S12). In addition, removal of the trisodium citrate from the reacted solution is guaranteed by the disappearance of the trisodium citrate signature (Appendix, Fig. S13), which also demonstrates efficiency of the sedimentation method as a washing procedure for this type of prepared particles.

The obtained LSPR bands are quite correct compared to other existing work on this topic [69,75–77], as the LSPR band is relatively intense and not very large (not so sharp either, despite a quite monodisperse gold particle size). The small silica particles exhibit a higher surface area (*i.e.* BET surface, Table 2) compared to the bigger silica particles. The 80 nm silica particles should then be covered with more gold particles than bigger silica particles and one would expect a higher LSPR intensity for these gold-silica particles, which is not the case. Indeed, the 80 nm silica particles tend to aggregate easily, which might lead to bonding in between gold grains from different silica particles and would negate the contribution of some of these gold grains. For the 600 nm silica particles, the LSPR band intensity is very reduced either for gold particles of 8.3 nm and 10.2 nm, probably because of the high intrinsic absorbance of the 600 nm silica particles (Appendix, Fig. S10). In addition, the LSPR peak position is slightly shifted to a higher wavelength compared to the gold particles intrinsic signature (Fig. 5). This effect might be explained by the interactions in between the close gold particles at the silica surface, and the surface curvature (in other words, the silica size), as the LSPR effect also depends on the propagation direction. Usually, the LSPR band is more intense when using gold particles of 10.3 nm instead of particles of 8.2 nm, which makes totally sense regarding the higher intrinsic LSPR intensities of these particles. Considering the LSPR band intensity, it seems better to use silica

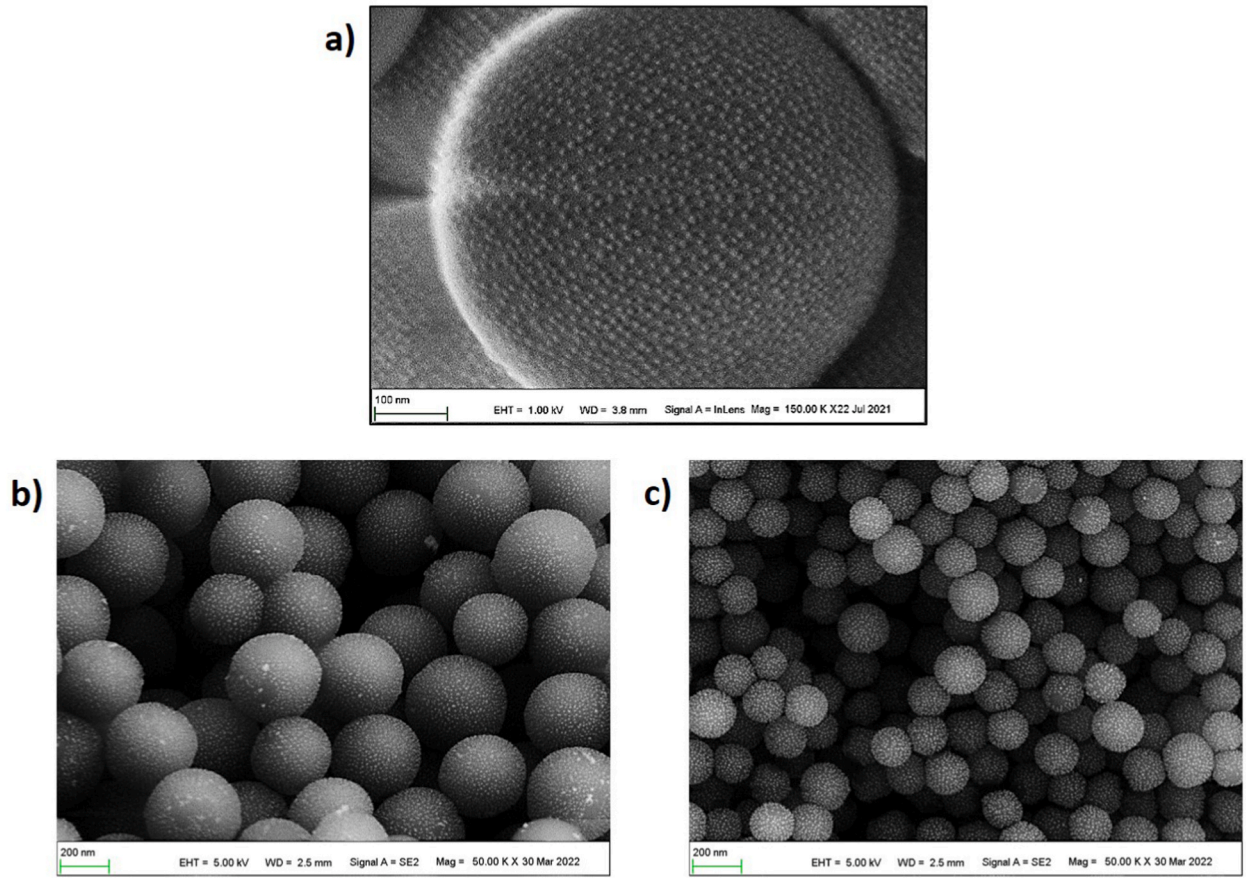

Fig. 8. SEM images of gold-silica LSPR nanoparticles obtained from heteroaggregation using 8 nm gold nanoparticles with silica nanoparticles with a size of 600 nm (a), 400 nm (b) and 150 nm (c) SEM pictures were taken with the as-synthesized silica-gold NPs, without additional metallization.

particles of a size below 600 nm.

To go further in explaining these phenomena, SEM observations were performed (Fig. 8(a–c)). Silica particles with a size 80 nm could not be observed in good conditions as they tend to aggregate a lot (Figs. 1 and 7). SEM analyses allow checking the spacing in between the grafted gold particles at the silica surface. Indeed, on the TEM pictures, there might be a confusion between grains from both sides of the particles (top and bottom) that are seen in transparency through the silica particles. Although SEM pictures are difficult to take due to charge effects during observation (different nature of the silica and gold materials), it was possible to get quite correct and descriptive pictures to help understanding the LSPR signatures.

For each type of silica particles, there is a regular spacing between the grafted gold grains. This may be attributed to the dispersant role of sodium citrate. The gold nanoparticles stay anchored at the silica surface even after removal of the trisodium citrate. From time to time, it is possible to find particles with holes at their surface (Fig. 8b & 8c), which might be attributed to the flow behavior when the silica particles enter fast into the gold particles solution (kind of a comet-like flow when entering the solution and the hole is the place without flow).

Coverage of the silica nanoparticles with the gold nanoparticles is dense and homogeneous for all sizes of silica particles. The gold grains are present on the silica particles with a good density and on large scale (Appendix, Fig. S14), which demonstrates the reproducible behavior and reliability of the preparation method using heteroaggregation.

4. Conclusions

The present work presented different prospective ways to produce silica nanoparticles covered by gold nanoparticles. The first approach of deposition precipitation (DP) method, consisting in the reactions of gold-seeding then gold-growing, showed a good density of seeds onto the silica nanoparticles. The use of heating method with microwave may be appropriate for preparing core-shell structures, due to a higher seeds density, but is not appropriate for achieving decorated particles with metallic nanoparticles without coalescence. Later, it appeared that the gold-growing procedure was of a major concern, as the use of the $NaBH_4$ compound in presence of gold chloride precursor was creating gold nanoparticles into the reaction medium. Careful attention should be given to the purification procedure, as the centrifugation method at medium speed is detaching the gold grains from the silica surface. Moreover, the

literature does not provide many data concerning the influence of the kinetics parameters (temperature and reaction time). It resulted in an inhomogeneous and non-reproducible coverage of the silica nanoparticles.

On the other hand, the heteroaggregation method allowed to show that the coverage of silica nanoparticles with gold nanoparticles is quite dense, homogeneous and reproducible. There is an influence of the silica particle size, or more precisely of the surface curvature, on the ability of the metallic particles to deposit onto the surface to be grafted. The purification procedure using washings with the sedimentation method is appropriate, as proven by the removal of trisodium citrate from the solution. The deposited gold grains stay individual without coalescence even after trisodium citrate removal. Heteroaggregation is an efficient method and the coverage of gold is even more reproducible and denser than other method using microfluidics functionalization [74].

The use of different silica particles sizes gave information about the LSPR performance of such silica-gold nanoparticles and the particle size is to be determined according to the desired application. Indeed, if the aim is to produce homogeneous single-crystal colloidal multilayers, it might be appropriate to choose silica particles of a size bigger than 300 nm to improve monodispersity and packing efficiency of such particles. On the other hand, if the application aims to develop a sensor based on a transmission method, it would be more appropriate to work with silica particles of a size below 200 nm that would result in a higher transmittance. Moreover, smaller silica particles are developing a higher surface area (in this work, up to roughly 10 times the one of bigger silica particles). We demonstrated that heteroaggregation is an efficient and reliable method to prepare gold-silica LSPR nanoparticles that exhibit appropriate and intense optical properties suitable for multiple applications.

Author contribution statement

Romain Trihan: Conceived and designed the experiments; Performed the experiments; Analyzed and interpreted the data; Wrote the paper. Oskar Bogucki, Martin Ihle, Bartosz Fetliński, Bartosz Janaszek: Contributed reagents, materials, analysis tools or data. Anna Kozlowska, Steffen Ziesche, Marcin Kieliszczyk, Marcin Kaczkan: Conceived and designed the experiments; Contributed reagents, materials, analysis tools or data. Fabrice Rossignol, Anne Aimable: Conceived and designed the experiments; Analyzed and interpreted the data; Wrote the paper.

Data availability statement

Data included in article/supp. material/referenced in article.

Declaration of competing interest

The authors declare that they have no known competing financial interests or personal relationships that could have appeared to influence the work reported in this paper.

Acknowledgments

Financial support of this work from the M-era. Net is gratefully acknowledged (contract number M-ERA. NET2/2019/8/2021). The postdoctoral position granting was also possible thanks to the National Centre for Scientific Research (CNRS) in France. We also would like to acknowledge the support of the National Centre for Research and Development (NCBR) in Poland. Acknowledgments to Prof. Vincent Sol and Prof. Vincent Chaleix for providing access to the microwave equipment used in this study. Acknowledgement to Dr. Amandine Magnaudeix for providing access to the Quickdrop equipment. Acknowledgements to Mr. Pierre Carles and Mrs. Eloise Hyvernaud for TEM and SEM observations, respectively.

Appendix A. Supplementary data

Supplementary data to this article can be found online at https://doi.org/10.1016/j.heliyon.2023.e15977.

References

[1] WMO/UNEP Intergovernmental Panel on Climate Change (IPCC), Report of the First Session of the WMP/UNEP Intergovernmental Panel on Climate Change (IPCC) IPCC-1, Nov. 1988, pp. 1–34.
[2] H. Tang, C. Zhu, G. Meng, N. Wu, Review—surface-Enhanced Raman scattering sensors for food safety and environmental monitoring, J. Electrochem. Soc. 165 (8) (2018) B3098–B3118.
[3] E. Bagheri, et al., Sensors design based on hybrid gold-silica nanostructures, Biosens. Bioelectron. 153 (Apr. 2020) 112054.
[4] V. Amendola, R. Pilot, M. Frasconi, O.M. Maragò, M.A. Iatì, Surface plasmon resonance in gold nanoparticles: a review, J. Phys. Condens. Matter 29 (20) (May 2017) 203002.
[5] A. Abbas, M.J. Linman, Q. Cheng, New trends in instrumental design for surface plasmon resonance-based biosensors, Biosens. Bioelectron. 26 (5) (Jan. 2011) 1815–1824.
[6] B. Prabowo, A. Purwidyantri, K.-C. Liu, Surface plasmon resonance optical sensor: a review on light source technology, Biosensors 8 (3) (Aug. 2018) 80.
[7] F. Xia, et al., Ultra-high sensitivity SPR fiber sensor based on multilayer nanoparticle and Au film coupling enhancement, Measurement 164 (Nov. 2020) 108083.

[8] H. Yuan, et al., Au nanoparticles as label-free competitive reporters for sensitivity enhanced fiber-optic SPR heparin sensor, Biosens. Bioelectron. 154 (Apr. 2020) 112039.
[9] J.-F. Masson, Surface plasmon resonance clinical biosensors for medical diagnostics, ACS Sens. 2 (1) (Jan. 2017) 16–30.
[10] S.K. Vashist, C.K. Dixit, B.D. MacCraith, R. O'Kennedy, Effect of antibody immobilization strategies on the analytical performance of a surface plasmon resonance-based immunoassay, Analyst 136 (21) (2011) 4431.
[11] J. Luo, J. Yao, Y. Lu, W. Ma, X. Zhuang, A silver nanoparticle-modified evanescent field optical fiber sensor for methylene blue detection, Sensors 13 (3) (Mar. 2013) 3986–3997.
[12] A.D. Kurdekar, et al., Fluorescent silver nanoparticle based highly sensitive immunoassay for early detection of HIV infection, RSC Adv. 7 (32) (2017) 19863–19877.
[13] P. Zrazhevskiy, M. Sena, X. Gao, Designing multifunctional quantum dots for bioimaging, detection, and drug delivery, Chem. Soc. Rev. 39 (11) (2010) 4326.
[14] X. Liu, et al., SPR quantitative analysis of direct detection of atrazine traces on Au-nanoparticles: nanoparticles size effect, Sens. Actuators, B 218 (Oct. 2015) 1–7.
[15] A. Rezabakhsh, R. Rahbarghazi, F. Fathi, Surface plasmon resonance biosensors for detection of Alzheimer's biomarkers; an effective step in early and accurate diagnosis, Biosens. Bioelectron. 167 (Nov. 2020) 112511.
[16] L.-Y. Niu, Q. Wang, J.-Y. Jing, W.-M. Zhao, Sensitivity enhanced D-type large-core fiber SPR sensor based on Gold nanoparticle/Au film co-modification, Opt Commun. 450 (Nov. 2019) 287–295.
[17] W.A. Murray, W.L. Barnes, Plasmonic materials, Adv. Mater. 19 (22) (Nov. 2007) 3771–3782.
[18] M. Edely, N. Delorme, D. Siniscalco, J.-F. Bardeau, Alternative strategy based on scanning probe lithography for patterning complex metallic nanostrutures on rigid or flexible substrates, Adv. Mater. Technol. 3 (11) (Nov. 2018) 1800134.
[19] J.-J. Li, D. Qiao, J. Zhao, G.-J. Weng, J. Zhu, J.-W. Zhao, Fluorescence turn-on sensing of L-cysteine based on FRET between Au-Ag nanoclusters and Au nanorods, Spectrochim. Acta. A. Mol. Biomol. Spectrosc. 217 (Jun. 2019) 247–255.
[20] N. Gandra, A. Abbas, L. Tian, S. Singamaneni, Plasmonic planet–satellite analogues: hierarchical self-assembly of gold nanostructures, Nano Lett. 12 (5) (May 2012) 2645–2651.
[21] A. Heuer-Jungemann, et al., The role of ligands in the chemical synthesis and applications of inorganic nanoparticles, Chem. Rev. 119 (8) (Apr. 2019) 4819–4880.
[22] J. Tang, et al., Silver-coated Si nanograss as highly sensitive surface-enhanced Raman spectroscopy substrates, Appl. Phys. A 96 (4) (Sep. 2009) 793–797.
[23] A. Upadhyaya, G. Rincón, Visible-light-active noble-metal photocatalysts for water disinfection: a review, J. Water Resour. Protect. 11 (10) (2019) 1207–1232.
[24] Y. Liu, H. Yuan, A.M. Fales, J.K. Register, T. Vo-Dinh, Multifunctional gold nanostars for molecular imaging and cancer therapy, Front. Chem. 3 (Aug) (2015).
[25] X. Huang, M.A. El-Sayed, Gold nanoparticles: optical properties and implementations in cancer diagnosis and photothermal therapy, J. Adv. Res. 1 (1) (Jan. 2010) 13–28.
[26] L. Rainville, M.-C. Dorais, D. Boudreau, Controlled synthesis of low polydispersity Ag@SiO2 core–shell nanoparticles for use in plasmonic applications, RSC Adv. 3 (33) (2013), 13953.
[27] S. Agnihotri, S. Mukherji, S. Mukherji, Size-controlled silver nanoparticles synthesized over the range 5–100 nm using the same protocol and their antibacterial efficacy, RSC Adv. 4 (8) (2014) 3974–3983.
[28] J. Choma, D. Jamioła, J. Ludwinowicz, M. Jaroniec, Deposition of silver nanoparticles on silica spheres and rods, Colloids Surf. A Physicochem. Eng. Asp. 411 (Oct. 2012) 74–79.
[29] A. Loiseau, V. Asila, G. Boitel-Aullen, M. Lam, M. Salmain, S. Boujday, Silver-based plasmonic nanoparticles for and their use in biosensing, Biosensors 9 (2) (Jun. 2019) 78.
[30] I. Zorić, M. Zäch, B. Kasemo, C. Langhammer, Gold, platinum, and aluminum nanodisk plasmons: material independence, subradiance, and damping mechanisms, ACS Nano 5 (4) (Apr. 2011) 2535–2546.
[31] S. De Marchi, S. Núñez-Sánchez, G. Bodelón, J. Pérez-Juste, I. Pastoriza-Santos, Pd nanoparticles as a plasmonic material: synthesis, optical properties and applications, Nanoscale 12 (46) (2020) 23424–23443.
[32] A.I. Bercea, et al., Adaptive gold/vanadium dioxide periodic arrays for infrared optical modulation, Appl. Surf. Sci. 585 (May 2022), 152592.
[33] M. Faraday, The bakerian lecture: experimental relations of gold (and other metals) to light, Phil. Trans. Roy. Soc. Lond. 147 (1857) 145–181.
[34] J. Turkevich, G. Garton, P.C. Stevenson, The color of colloidal gold, J. Colloid Sci. 9 (Jan. 1954) 26–35.
[35] G. Frens, Controlled nucleation for the regulation of the particle size in monodisperse gold suspensions, Nat. Phys. Sci. 241 (105) (Jan. 1973) 20–22.
[36] X. Ji, X. Song, J. Li, Y. Bai, W. Yang, X. Peng, Size control of gold nanocrystals in citrate reduction: the third role of citrate, J. Am. Chem. Soc. 129 (45) (Nov. 2007) 13939–13948.
[37] N.T.K. Thanh, N. Maclean, S. Mahiddine, Mechanisms of nucleation and growth of nanoparticles in solution, Chem. Rev. 114 (15) (Aug. 2014) 7610–7630.
[38] B.J. Jankiewicz, D. Jamiola, J. Choma, M. Jaroniec, Silica–metal core–shell nanostructures, Adv. Colloid Interface Sci. 170 (1–2) (Jan. 2012) 28–47.
[39] J.F. Li, et al., Surface analysis using shell-isolated nanoparticle-enhanced Raman spectroscopy, Nat. Protoc. 8 (1) (Jan. 2013) 52–65.
[40] V.K.T. Ngo, H.P.U. Nguyen, T.P. Huynh, N.N.P. Tran, Q.V. Lam, T.D. Huynh, Preparation of gold nanoparticles by microwave heating and application of spectroscopy to study conjugate of gold nanoparticles with antibody *E. coli* O157:H7, Adv. Nat. Sci. Nanosci. Nanotechnol. 6 (3) (Jul. 2015) 35015.
[41] S.K. Seol, D. Kim, S. Jung, Y. Hwu, Microwave synthesis of gold nanoparticles: effect of applied microwave power and solution pH, Mater. Chem. Phys. 131 (1–2) (Dec. 2011) 331–335.
[42] D.G. Duff, A. Baiker, P.P. Edwards, A new hydrosol of gold clusters. 1. Formation and particle size variation, Langmuir 9 (9) (Sep. 1993) 2301–2309.
[43] M.N. Martin, J.I. Basham, P. Chando, S.-K. Eah, Charged gold nanoparticles in non-polar solvents: 10-min synthesis and 2D self-assembly, Langmuir 26 (10) (May 2010) 7410–7417.
[44] J. Piella, N.G. Bastús, V. Puntes, Size-controlled synthesis of sub-10-nanometer citrate-stabilized gold nanoparticles and related optical properties, Chem. Mater. 28 (4) (Feb. 2016) 1066–1075.
[45] C.J. Murphy, et al., Anisotropic metal nanoparticles: synthesis, assembly, and optical applications, J. Phys. Chem. B 109 (29) (Jul. 2005) 13857–13870.
[46] C. Loo, et al., Nanoshell-enabled photonics-based imaging and therapy of cancer, Technol. Cancer Res. Treat. 3 (1) (Feb. 2004) 33–40.
[47] F. Tam, G.P. Goodrich, B.R. Johnson, N.J. Halas, Plasmonic enhancement of molecular fluorescence, Nano Lett. 7 (2) (Feb. 2007) 496–501.
[48] S.E. Skrabalak, et al., Gold nanocages: synthesis, properties, and applications, Acc. Chem. Res. 41 (12) (Dec. 2008) 1587–1595.
[49] D. Chateau, et al., From gold nanobipyramids to nanojavelins for a precise tuning of the plasmon resonance to the infrared wavelengths: experimental and theoretical aspects, Nanoscale 7 (5) (2015) 1934–1943.
[50] A.M. Fales, H. Yuan, T. Vo-Dinh, Silica-coated gold nanostars for combined surface-enhanced Raman scattering (SERS) detection and singlet-oxygen generation: a potential nanoplatform for theranostics, Langmuir 27 (19) (Oct. 2011) 12186–12190.
[51] H. Yuan, C.G. Khoury, H. Hwang, C.M. Wilson, G.A. Grant, T. Vo-Dinh, Gold nanostars: surfactant-free synthesis, 3D modelling, and two-photon photoluminescence imaging, Nanotechnology 23 (7) (Feb. 2012) 75102.
[52] M. Ben Haddada, et al., Optimizing the immobilization of gold nanoparticles on functionalized silicon surfaces: amine- vs thiol-terminated silane, Gold Bull. 46 (4) (Dec. 2013) 335–341.
[53] C.-H. Lee, T.-S. Lin, C.-Y. Mou, Mesoporous materials for encapsulating enzymes, Nano Today 4 (2) (Apr. 2009) 165–179.
[54] X. Cattoën, et al., Click approaches in sol–gel chemistry, J. Sol. Gel Sci. Technol. 70 (2) (2013) 245–253.
[55] W. Stöber, A. Fink, E. Bohn, Controlled growth of monodisperse silica spheres in the micron size range, J. Colloid Interface Sci. 26 (1) (Jan. 1968) 62–69.
[56] P. Jiang, J.F. Bertone, K.S. Hwang, V.L. Colvin, Single-crystal colloidal multilayers of controlled thickness, Chem. Mater. 11 (8) (Aug. 1999) 2132–2140.
[57] K.W. Shah, T. Sreethawong, S.-H. Liu, S.-Y. Zhang, L.S. Tan, M.-Y. Han, Aqueous route to facile, efficient and functional silica coating of metal nanoparticles at room temperature, Nanoscale 6 (19) (Jul. 2014) 11273–11281.

[58] Z. Wu, J. Liang, X. Ji, W. Yang, Preparation of uniform Au@SiO2 particles by direct silica coating on citrate-capped Au nanoparticles, Colloids Surf. A Physicochem. Eng. Asp. 392 (1) (Dec. 2011) 220–224.
[59] C. Graf, D.L.J. Vossen, A. Imhof, A. van Blaaderen, A general method to coat colloidal particles with silica, Langmuir 19 (17) (Aug. 2003) 6693–6700.
[60] C. Graf, A. van Blaaderen, Metallodielectric colloidal Core−Shell particles for photonic applications, Langmuir 18 (2) (Jan. 2002) 524–534.
[61] J. Choma, A. Dziura, D. Jamioła, P. Nyga, M. Jaroniec, Preparation and properties of silica–gold core–shell particles, Colloids Surf. A Physicochem. Eng. Asp. 373 (1–3) (Jan. 2011) 167–171.
[62] S.T. Kochuveedu, T. Son, Y. Lee, M. Lee, D. Kim, D.H. Kim, Revolutionizing the FRET-based light emission in core-shell nanostructures via comprehensive activity of surface plasmons, Sci. Rep. 4 (1) (May 2015) 4735.
[63] J. Asselin, M.L. Viger, D. Boudreau, Metal-Enhanced fluorescence and FRET in multilayer core-shell nanoparticles, Adv. Chem. 2014 (Jun. 2014) 1–16.
[64] L.M. Liz-Marzán, M. Giersig, P. Mulvaney, Synthesis of nanosized Gold−Silica Core−Shell particles, Langmuir 12 (18) (Jan. 1996) 4329–4335.
[65] N. Phonthammachai, et al., Synthesis of contiguous Silica−Gold Core−Shell structures: critical parameters and processes, Langmuir 24 (9) (May 2008) 5109–5112.
[66] J.C.Y. Kah, et al., Synthesis of gold nanoshells based on the depositionprecipitation process, Gold Bull. 41 (1) (Mar. 2008) 23–36.
[67] P. Khurana, S. Thatai, J. Boken, S. Prasad, D. Kumar, Development of promising surface enhanced Raman scattering substrate: freckled SiO2@Au nanocomposites, Microchem. J. 122 (Sep. 2015) 45–49.
[68] M.R. Rasch, K.V. Sokolov, B.A. Korgel, Limitations on the optical tunability of small diameter gold nanoshells, Langmuir 25 (19) (Oct. 2009) 11777–11785.
[69] R. Ashayer, S.H. Mannan, S. Sajjadi, Synthesis and characterization of gold nanoshells using poly(diallyldimethyl ammonium chloride), Colloids Surf. A Physicochem. Eng. Asp. 329 (3) (Nov. 2008) 134–141.
[70] H. Li, X. Ma, J. Dong, W. Qian, Development of methodology based on the formation process of gold nanoshells for detecting hydrogen peroxide scavenging activity, Anal. Chem. 81 (21) (Nov. 2009) 8916–8922.
[71] S.J. Oldenburg, R.D. Averitt, S.L. Westcott, N.J. Halas, Nanoengineering of optical resonances, Chem. Phys. Lett. 288 (2–4) (May 1998) 243–247.
[72] P. Dobrowolska, A. Krajewska, M. Gajda-Rączka, B. Bartosewicz, P. Nyga, B. Jankiewicz, Application of Turkevich method for gold nanoparticles synthesis to fabrication of SiO2@Au and TiO2@Au core-shell nanostructures, Materials 8 (6) (May 2015) 2849–2862.
[73] X. Ma, W. Qian, Phenolic acid induced growth of gold nanoshells precursor composites and their application in antioxidant capacity assay, Biosens. Bioelectron. 26 (3) (Nov. 2010) 1049–1055.
[74] N. Hassan, V. Cabuil, A. Abou-Hassan, Continuous multistep microfluidic assisted assembly of fluorescent, plasmonic, and magnetic nanostructures, Angew. Chem., Int. Ed. 52 (7) (Feb. 2013) 1994–1997.
[75] J. Xue, C. Wang, Z. Ma, A facile method to prepare a series of SiO2@Au core/shell structured nanoparticles, Mater. Chem. Phys. 105 (2–3) (Oct. 2007) 419–425.
[76] Y.-L. Shi, T. Asefa, Tailored Core−Shell−Shell nanostructures: sandwiching gold nanoparticles between silica cores and tunable silica shells, Langmuir 23 (18) (Aug. 2007) 9455–9462.
[77] L. Zhang, Y.-G. Feng, L.-Y. Wang, J.-Y. Zhang, M. Chen, D.-J. Qian, Comparative studies between synthetic routes of SiO2@Au composite nanoparticles, Mater. Res. Bull. 42 (8) (Aug. 2007) 1457–1467.
[78] X. Ji, et al., Bifunctional gold nanoshells with a superparamagnetic iron Oxide−Silica core suitable for both MR imaging and photothermal therapy, J. Phys. Chem. C 111 (17) (May 2007) 6245–6251.
[79] N.G. Bastús, J. Comenge, V. Puntes, Kinetically controlled seeded growth synthesis of citrate-stabilized gold nanoparticles of up to 200 nm: size focusing versus ostwald ripening, Langmuir 27 (17) (Sep. 2011) 11098–11105.